Astrophysical Dynamics: From Stars to Galaxies
Proceedings IAU Symposium No. 271, 2010
N.H. Brummell, A.S. Brun, M. S. Miesch & Y. Ponty, eds.

doi:10.1017/S1743921311017509

On the formation of ring galaxies

Yu-Ting Wu[1] and Ing-Guey Jiang[2]

[1]Department of Physics, National Tsing-Hua University,
Hsinchu, Taiwan 30013, R. O. C.
email: d9622814@oz.nthu.edu.tw

[2]Department of Physics and Institute of Astronomy, National Tsing-Hua University,
Hsinchu, Taiwan 30013, R. O. C.
email: jiang@phys.nthu.edu.tw

Abstract. The formation scenario of ring galaxies is addressed in this paper. We focus on the P-type ring galaxies presented in Madore, Nelson & Petrillo (2009), particularly on the axis-symmetric ones. Our simulations show that a ring can form through the collision of disc and dwarf galaxies, and the locations, widths, and density contrasts of the ring are well determined. We find that a ring galaxy such as AM 2302-322 can be produced by this collision scenario.

Keywords. galaxies: formation, galaxies: interactions, galaxies: kinematics and dynamics

1. Introduction

Ring galaxies, a peculiar class of galaxies, contain various ring-like structures with or without clumps, nuclei, companions or spokes. For example, the famous Cartwheel galaxy was first discovered by Zwicky (1941) and shows an outer ring, an inner ring, a nucleus and spokes (Theys & Spiegel 1976; Fosbury & Hawarden 1977; Higdon 1995). According to the morphology of ring galaxies, Few & Madore (1986) studied 69 ring galaxies in the southern hemisphere and developed a classification scheme. The ring galaxies are classified into two main classes, the O-type and P-type galaxies. The O-type galaxies have a central nucleus and smooth regular ring, while P-type systems often contain an offset nucleus and a knotty ring.

As more and more observational data on ring galaxies have been obtained (Arp & Madore 1987; Bushouse & Standford 1992; Marston & Appleton 1995; Elmegreen & Elmegreen 2006; Madore et. al. 2009), three dominant theories have been proposed to explain the formation and evolution of ring galaxies: the collision scenario, the resonance scenario and the accretion scenario. In the collision scenario suggested by Lynds & Toomre (1976), ring galaxies are formed after a head-on collision between an intruder galaxy and a disk galaxy. The formation of the Cartwheel galaxy is thought to be a prototype of this scenario. Furthermore, from the observational statistics by Few & Madore (1986), P-type galaxies have an excess of companions and can be considered to be formed by the collision scenario. In the resonance scenario, ring-like patterns are formed by gas accumulation at Lindblad resonances which respond to external perturbations, such as a bar or an oval. O-type galaxies with central nucleus and no obvious companions are thought to experience the resonance formation process, for instance, IC 4214 (Buta *et al.* 1999). For the third scenario, accretion scenario, it was proposed to explain the origin of the polar ring galaxies. The polar ring galaxies contain the host galaxies and the outer rings with gas and stars which orbit nearly perpendicular to the plane of the host galaxies. This type of galaxy is believed to be formed when the material from another galaxy or intergalactic medium is accreted onto the host galaxy. A possible prototype of this scenario is the formation of NGC 4650A (Bournaud & Combes 2003).

Recently, a catalog and imaging atlas of 104 P-type galaxies are presented in Madore, Nelson & Petrillo (2009). Our goal is to examine the formation of P-type ring galaxies shown in that catalog. We will determine the locations, widths, and density contrasts of rings and study the evolution of these quantities. In this project, we focus on axis-symmetric rings as in AM 2302-322.

2. The Model

In this study, the target and the intruder are assumed to be a disc galaxy and a dwarf galaxy respectively. We investigate the response of collisions between the target disc galaxy, consisting of the stellar disc and the dark matter halo, and the less massive dwarf galaxy, containing the dark matter halo and the stellar component. The stellar disc and the dark matter halo of the target galaxy have the same density profiles as in Hernquist (1993). The intruder dwarf galaxy comprises the dark matter halo and stellar part with Plummer spheres (Binney & Tremaine 1987; Read *et al.* 2006). The simulation are carried out with the parallel tree-code GADGET (Springel, Yoshida & White 2001) and the softening length are set to be 0.15 kpc and 0.09 kpc for the target disc galaxy and the intruder dwarf galaxy, respectively.

The initial positions of particles can be easily determined according to the above given density profiles. However, assigning initial velocities to each particle will need more complicated techniques. For the spherically symmetric systems, such as the dark matter halo of the disc galaxy and both components of the dwarf galaxy, the initial velocities are calculated from the phase-space distribution functions which can be obtained from Eddington's formula (Binney & Tremaine 1987). For non-spherically symmetric systems, such as the stellar disc, the velocities are determined from the moments of the collisionless Boltzmann equation as in Hernquist (1993) because the analytical phase-space distribution function is not available.

Throughout this paper, the following system of units is used: the gravitational constant G is 43,007.1, the unit of length is 3 kpc, the unit of mass is $10^{10} M_{\odot}$ and the unit of time is 5.09×10^9 yr. Using the above units, for the disc galaxy, the disc mass, M_d, is 5.6, the disc radial scale length, h, is 3.5, the disc vertical scale length, z_0, is 0.7, the halo mass, M_h, is 32.48, the halo core radius, r_c, is 3.5 and the halo tidal radius, r_t, is 35.0. The disc galaxy has a total of 340,000 particles, i.e. 290,000 dark matter particles and 50,000 stellar particles in the disc. The dynamical time, T_{dyn}, can be defined by the velocity, $v_{1/2}$, of a test particle at disc's half-mass radius, $R_{1/2} = 5.95$, that is $T_{dyn} \equiv 2\pi R_{1/2}/v_{1/2} = 0.174$, where $v_{1/2} = 214.77$.

We combine the dark matter halo and the stellar disc to set up the disc galaxy after constructing these two components independently. These two components of the disc galaxy influence each other and then approach to a new equilibrium. According to the virial theorem, when the disc galaxy is in equilibrium, the value of $2K/|U|$ should be around one, where K and U are total kinetic energy and total potential energy, respectively. Hereafter, $2K/|U|$ is called the *virial ratio*. The disc galaxy approaches a new equilibrium at $t = 15T_{dyn}$ and the energy conservation is fulfilled because the total energy variation is 0.082 per cent. Hence, the disc galaxy at $t = 15T_{dyn}$ will be used to represent the target disc galaxy at the beginning of the collision simulation.

For the dwarf galaxy, the total mass is 9.52, which is a quarter of the mass of the disc galaxy, and the mass to light ratio is 5. The scale lengths of the dark matter halo and the stellar component are 3.0 and 1.5 respectively. The total number of particles is 85,000, containing 68,000 dark matter particles and 17,000 stellar particles. The mass of each particle in our simulation is the same. Because the dark matter halo and the

https://doi.org/10.1017/S1743921311017509 Published online by Cambridge University Press

stellar component of the dwarf galaxy are both spherically symmetric and can be set up together, the whole dwarf galaxy with two components is in equilibrium initially. This dwarf galaxy will be the intruder galaxy in the collision simulation.

3. The Evolution

The target disc galaxy and the dwarf galaxy are set up as mentioned previously. The initial separation of these two galaxies is 200, which is far enough to make sure two galaxies are well separated, and the initial relative velocity $v_i = 286.2$. To fix the center of mass of the collision system at the origin, the disc galaxy is located at $(x, y, z) = (0, 0, -40)$ with $(v_x, v_y, v_z) = (0, 0, 57.24)$ and the dwarf galaxy is located at $(x, y, z) = (0, 0, 160)$ with $(v_x, v_y, v_z) = (0, 0, -228.96)$.

To have more detail about the evolution of the galaxies in the simulation, the time interval between each snapshot is set to be $T_s = T_{dyn}/2$. The virial ratio, $2K/|U|$, of the collision system as a function of time during $t = 0$ - $80T_s$ is shown in Fig. 1 (a). Owing to the strong interaction between the disc galaxy and the dwarf galaxy during $t = 6$ - $22T_s$, the virial ratio goes away from one. The first peak and the second peak of $2K/|U|$ are around $t = 7T_s$ and $t = 21T_s$, respectively, while the minimum of $2K/|U|$ is around $t = 15T_s$.

In addition, Fig. 1 (b) shows the centers of mass of both galaxies during the collision. The disc and dwarf galaxies have a close encounter at $t = 7T_s$ and then separate at $t = 15T_s$. After $6T_s$, i.e. at $t = 21T_s$, two galaxies approach one another again because of the gravitational force. In a comparison of Fig. 1 (a) and (b), it is clear that two peaks of $2K/|U|$ at $t = 7T_s$ and $t = 21T_s$ in Fig. 1 (a) imply two encounters between the disc galaxy and the dwarf galaxy at these times. Moreover, the minimum of $2K/|U|$ at $t = 15T_s$ between two peaks of $2K/|U|$ infers that there is a separation between two encounters.

Fig. 2 shows the time evolution of the stellar disc and the stellar component of the dwarf galaxy in the edge-on view. Initially, two galaxies are separated by 200. During the early phases of the encounter, from $t = 0$ to $t = 6T_s$, two galaxies approach each other and then encounter at $t = 7T_s$. Later on, the gravitational force from the dwarf galaxy warps the stellar disc upward and downward between $t = 8T_s$ to $t = 21T_s$. Furthermore, since many particles of the dwarf galaxy escape from the center of the dwarf galaxy, the dwarf galaxy starts to expand after the encounter. Consequently, the stellar disc becomes a layered appearance at $t = 24T_s$ and its thickness increases with time, e.g. at $t = 27T_s$. Most particles of the dwarf galaxy are concentrated around the stellar disc, but some of them extend to a distance about 300.

4. The Ring

Fig. 3 (a) shows the surface density of all stellar particles projected along the collision axis (i.e. onto x-y plane) in the collision system and the fitted disc surface density profile at $t = 0$ and after the encounters, at $t = 7T_s$, $t = 8T_s$ and $t = 9T_s$. To obtain an analytic curve to fit the surface density profiles, we first integrate the density profile of the disc to yield the surface density as

$$\Sigma(R) = \frac{M_d}{2\pi h^2} \exp\left(\frac{-R}{h}\right). \tag{4.1}$$

https://doi.org/10.1017/S1743921311017509 Published online by Cambridge University Press

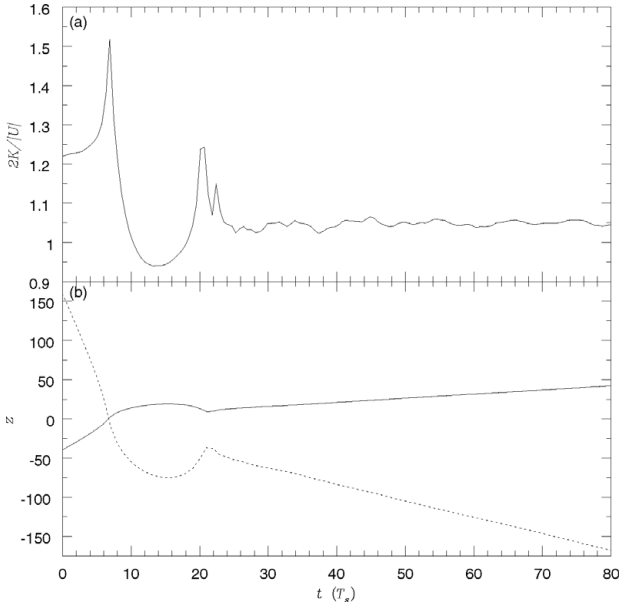

Figure 1. The evolution of the collision simulation. (a) The virial ratio $2K/|U|$ of the collision system as a function of time. (b) The center of mass of each galaxy in the collision simulation during the whole simulation time. The solid line and the dotted line are for the locations of the disc galaxy and the dwarf galaxy, respectively. The unit of t is $T_s = T_{dyn}/2$.

We further modify it to be

$$\Sigma(R) = \alpha \frac{M_d}{2\pi h^2} \exp\left(\frac{-\beta R}{h}\right), \tag{4.2}$$

where two additional fitting parameters, α and β, are introduced. The best-fitting parameter set (α, β) is determined by minimizing χ^2 (Wall & Jenkins 2003) as

$$\chi^2 = \sum_{i=1}^{k} \frac{(Q_i - E_i)^2}{E_i} \tag{4.3}$$

where Q_i is the surface density at a radius R_i and E_i is the $\Sigma(R_i)$ with the fitting parameter set (α, β). In the χ^2 fitting procedure, we neglect the surface density beyond the radius R_{end}, where the surface density Q_{end} is zero.

In Fig. 3 (a), the filled circles, open circles, crosses and open triangles represent the surface density at $t = 7$, $t = 8T_s$, $t = 9T_s$ and $t = 10T_s$, respectively. The solid, dot, short-dashed and long-dashed lines are the best-fitting profiles with the parameter set $(\alpha, \beta) = (3.2, 1.5)$, $(2.1, 1.1)$ and $(1.7, 1.0)$, $(1.4, 0.9)$ for filled circles, open circles, crosses and open triangles, respectively. Fig. 3 (b) shows the same thing on a logarithmic scale. From Fig. 3 (a) and (b), it is clear that after the encounter, a ring-like feature is evident at $t = 7T_s$ and then propagates outward as an expanding ring after $t = 7T_s$. In addition, the rings are also produced at $t = 12T_s$ to $t = 15T_s$ and $t = 21T_s$ to $t = 22T_s$ due to the perturbation after the first encounter at $t = 7T_s$ and the second encounter at $t = 21T_s$. The best-fitting parameter sets, (α, β), at these times are shown in Table 1.

To determine the position of the ring, the density contrast is defined as $\frac{\Delta\Sigma(R)}{\Sigma(R)}$, where $\Delta\Sigma(R)$ is the difference between the surface density and the best-fitting profile at a radius R, i.e. $\Sigma(R)$. The $\Delta\Sigma(R)$ and the density contrast, $\frac{\Delta\Sigma(R)}{\Sigma(R)}$, as a function of radius R at

https://doi.org/10.1017/S1743921311017509 Published online by Cambridge University Press

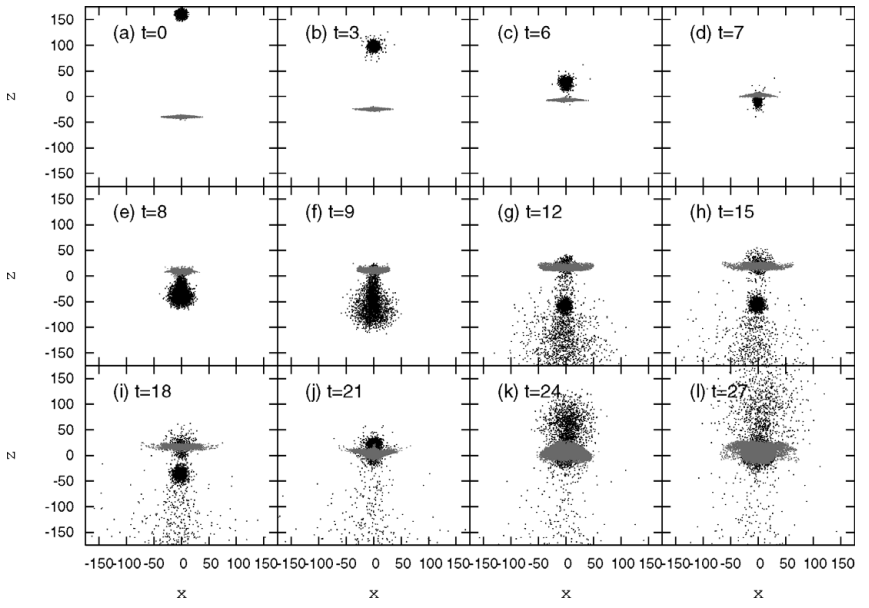

Figure 2. The time evolution of the stellar disc and the stellar component of the dwarf galaxy in the edge-on view. The gray dots and the black dots represent the stellar disc and the stellar part of the dwarf galaxy, respectively. The unit of time is $T_s = T_{dyn}/2$

.

Table 1. The best-fitting parameter set (α, β) of the surface densities.

	(α, β)	a	b	L	W
$t = 7T_s$	(3.2, 1.5)	3.55	4.35	3.95	0.80
$t = 8T_s$	(2.1, 1.1)	14.05	17.25	15.65	3.20
$t = 9T_s$	(1.7, 1.0)	21.35	27.25	24.30	5.90
$t = 10T_s$	(1.4, 0.9)	27.45	37.25	32.35	9.80
$t = 12T_s$	(1.3, 0.9)	17.25	20.05	18.65	2.80
$t = 13T_s$	(1.3, 0.9)	19.75	23.05	21.40	3.30
$t = 14T_s$	(1.4, 1.0)	21.85	29.45	25.65	7.60
$t = 15T_s$	(1.4, 1.0)	23.15	30.85	27.00	7.70
$t = 21T_s$	(2.1, 1.1)	9.55	12.15	10.85	2.60
$t = 22T_s$	(2.0, 1.0)	19.95	27.15	23.55	7.20

$t = 7T_s$, $t = 8T_s$, $t = 9T_s$ and $t = 10T_s$ are shown in Fig. 3 (c) and (d), respectively. The different symbols (i.e. the filled circles, open circles, crosses and open triangles) represent the $\Delta\Sigma(R)$ and the density contrast, $\frac{\Delta\Sigma(R)}{\Sigma(R)}$, at different times as described in Fig. 3 (a).

From the density contrast as shown in Fig. 3 (d), we can determined the region around a ring-like feature in which all the density contrasts are larger than zero. Then, the average of density contrasts in this region, $(\frac{\Delta\Sigma}{\Sigma})_{av}$, can be calculated and the corresponding radius a and b are determined at which the density contrast reaches $(\frac{\Delta\Sigma}{\Sigma})_{av}$. Therefore,

https://doi.org/10.1017/S1743921311017509 Published online by Cambridge University Press

the boundaries of the ring are defined to be at radius a and b. The location (L) of the ring is $L = \frac{a+b}{2}$ and the width (W) of the ring is $W = |b - a|$.

The boundaries, the location, and the width of the ring at different simulation times are shown in Table 1.

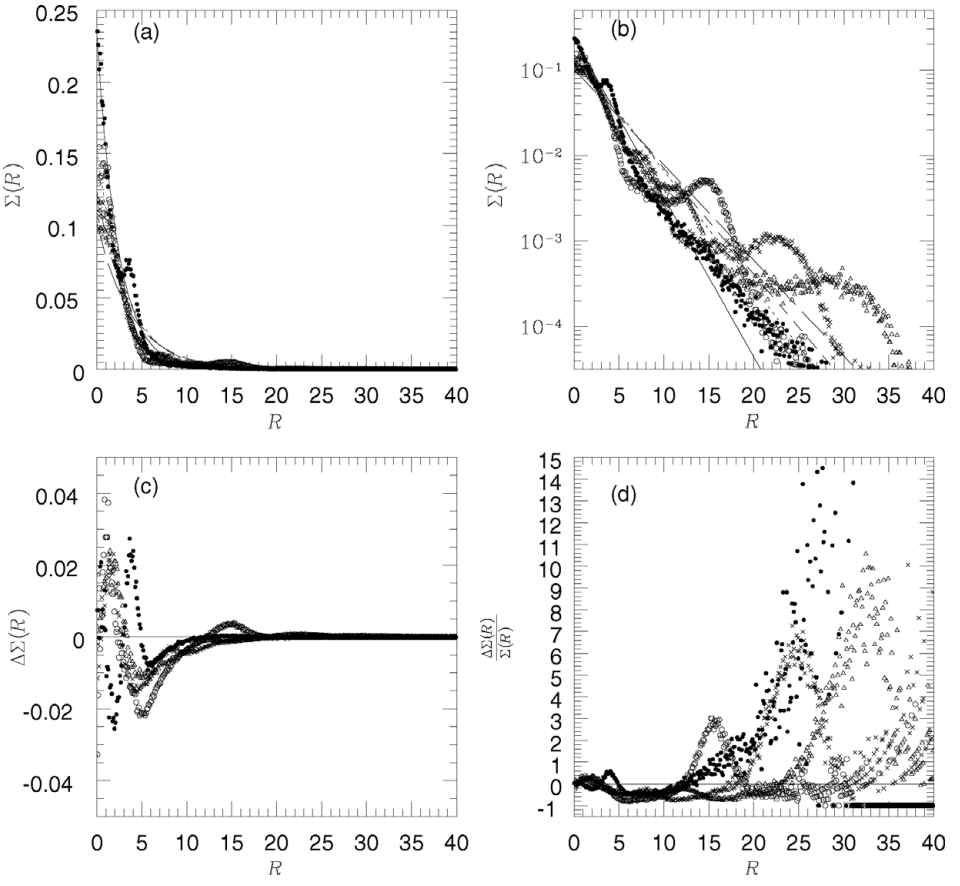

Figure 3. (a) The surface density profiles and the best-fitting profiles at the different times. The filled circles, open circles, crosses and open triangles represent the surface density profiles at $t = 7T_s$, $t = 8T_s$, $t = 9T_s$ and $t = 10T_s$, respectively. The solid, dot, short-dashed and long–dashed lines are the best-fitting profiles for the above four different kinds of points, respectively. (b) The same thing as shown in (a) on a logarithmic scale. (c) $\Delta\Sigma(R)$, which is the difference between the surface density and the best-fitting profile, as a function of radius at $t = 7T_s$ (filled circles), $t = 8T_s$ (open circles), $t = 9T_s$ (crosses) and $t = 10T_s$ (open triangles). (d) The density contrast as a function of radius at $t = 7T_s$ (filled circles), $t = 8T_s$ (open circles), $t = 9T_s$ (crosses) and $t = 10T_s$ (open triangles).

Fig. 4 shows the characteristics of the ring at different simulation times. The average of the density contrast in the ring region as a function of time and the location of the ring as a function of time are plotted in Fig. 4 (a) and (b). Fig. 4 (b) shows three generation rings form at $t = 7T_s$, $t = 12T_s$ and $t = 21T_s$, and then move outward. As the ring keeps going outward, the average of density contrast increases as shown in Fig. 4 (a). In addition, the width of the ring as a function of time is displayed in Fig. 4 (c) and shows that the width of the ring is wider when the density contrast is higher. When the ring is cut with lines along radial directions into 360 equal-size angular bins, the average number of particles in angular bins is shown in Fig. 4 (d), where error bars show the variation

https://doi.org/10.1017/S1743921311017509 Published online by Cambridge University Press

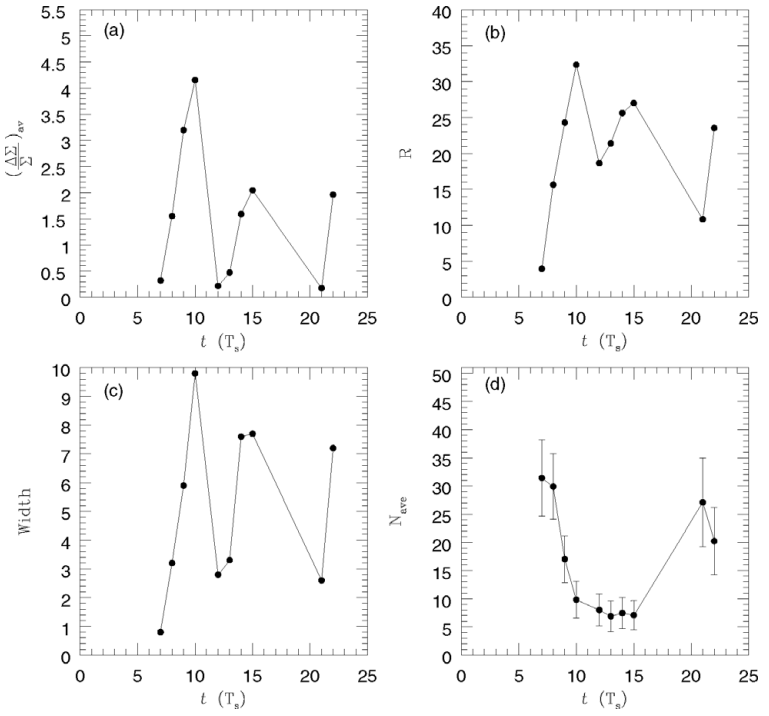

Figure 4. (a) The average of the density contrast in the ring region as a function of time. (b) The location of the ring as a function of time. (c) The width of the ring as a function of time. (d) The average number of particles in angular bins. The error bar shows the variation in different angular bins.

in different angular bins. This panel confirms that the structure of the ring at different times is smooth without a large clump.

5. Concluding Remarks

A catalog and imaging atlas of P-type galaxies are presented by Madore, Nelson & Petrillo (2009) recently. Most P-type ring galaxies have been interpreted as the result of a head-on collision between a disc galaxy and an intruder galaxy, i.e. the collision scenario. We have performed the simulation of the collision between a disc galaxy and an intruder dwarf galaxy to test the collision scenario, and developed a method to determine the location, width and density contrast of a ring structure. Our simulation shows that a ring-like feature could form after the encounters between two galaxies. Because the dwarf galaxy gets destroyed, we produce a ring galaxy without companions. In comparing our simulation to the AM 2302-322 ring galaxy (Madore, Nelson & Petrillo 2009), we find that the density contrast of the ring in our simulation at $t = 7T_s$ is in the same order as the density contrast of AM 2302-322. We conclude that a P-type ring galaxy, such as AM 2302-322, can be formed through the galactic collisions.

References

Arp H. C. & Madore B. F. 1987, *A Catalogue of Southern Peculiar Galaxies and Associations, Cambridge Univ. Press, Cambridge*

Binney J. & Tremaine S. 1987, *Galactic Dynamics (Princeton Univ. Press)*

https://doi.org/10.1017/S1743921311017509 Published online by Cambridge University Press

Bournaud F. & Combes F. 2003, *A&A*, 401, 817
Bushouse H. A. & Stanford S. A. 1992, *ApJS*, 79, 213
Buta R., Purcell G. B., Cobb M. L., Crocker D. A., Rautiainen P., & Salo H. 1999, *AJ*, 117, 778
Elmegreen D. M. & Elmegreen B. G. 2006, *ApJ*, 651, 676
Few J. M. A. & Madore B. F. 1986, *MNRAS*, 222, 673
Fosbury R. A. E. & Hawarden T. G. 1977, *MNRAS*, 178, 473
Hernquist L. 1993, *ApJS*, 86, 389
Higdon J. L. 1995, *ApJ* 455, 524
Lynds R. & Toomre A. 1976, *ApJ*, 209, 382
Madore B. F., Nelson E., & Petrillo K. 2009, *ApJS*, 181, 572
Marston A. P. & Appleton P. N. 1995, *AJ*, 109, 1002
Read, J. I., Wilkinson, M. I., Evans, N. W., Gilmore, G., & Kleyna, J. T. 2006, *MNRAS*, 367, 387
Springel V., Yoshida N., & White S. D. M.. 2001, *NewA*, 6, 79
Theys J. C. & Spiegel E. A. 1976, *ApJ*, 208, 650
Wall J. V. & Jenkins C. R. 2003, *Practical Statistics for Astronomers, Cambridge Univ. Press, Cambridge*
Zwicky F. 1941, *Applied Mechanics (von Kármán volume)*, p.137

Discussion

F. Combes: In your ring simulations, should you take into account the star formation triggered by the ring wave? the contrast of the ring could be much stronger.

Y.-T. Wu: If we consider the star formation in the simulations, it might increase the density contrast of the ring. However, the simulations here can already explain some observational data.

https://doi.org/10.1017/S1743921311017509 Published online by Cambridge University Press